Research Article | Vol. 9, No. 3 | 1 Mar 2019 | OPTICAL MATERIALS EXPRESS 1271
Optical Materials EXPRESS

Nonlinear optical properties of polycrystalline silicon core fibers from telecom wavelengths into the mid-infrared spectral region

H. REN,[1] L. SHEN,[1,2,*] D. WU,[1] O. AKTAS,[1] T. HAWKINS,[3] J. BALLATO,[3] U. J. GIBSON,[4,5] AND A. C. PEACOCK[1]

[1] *Optoelectronics Research Centre, University of Southampton, Southampton, SO17 1BJ, UK*
[2] *Wuhan National Laboratory for Optoelectronics, School of Optical and Electronic Information, Huazhong University of Science and Technology, Wuhan 430074, Hubei, China*
[3] *Center for Optical Materials Science and Engineering Technologies (COMSET) and Department of Materials Science and Engineering, Clemson University, Clemson, SC 29634, USA*
[4] *Department of Physics and Porelabs, Norwegian University of Science and Technology, N-7491 Trondheim, Norway*
[5] *Department of Applied Physics, KTH Royal Institute of Technology, Stockholm 10044, Sweden*
[*] *L.Shen@soton.ac.uk*

Abstract: Polycrystalline silicon core fibers (SCFs) fabricated via the molten core drawing (MCD) method are emerging as a flexible optoelectronic platform. Here, the optical transmission properties of MCD SCFs that have been tapered down to a few micrometer-sized core dimensions are characterized from the telecom band to the mid-infrared spectal regime. The SCFs exhibit low linear losses on the order of a few dB/cm over the entire wavelength range. Characterization of the two-photon absorption coefficient (β_{TPA}) and nonlinear refractive index (n_2) of the SCFs reveals values consistent with previous measurements of single crystal silicon materials, indicating the high optical quality of the polysilicon core material. The high nonlinear figure of merit obtained for wavelengths above 2 μm highlight the potential for these fibers to find application in infrared nonlinear photonics.

1. Introduction

Nonlinear silicon photonics has attracted growing interest in the past two decades and numerous nonlinear effects in silicon materials have been demonstrated for a wide variety of applications including wavelength conversion, signal amplification and broadband supercontinuum generation [1]. Most of these nonlinear effects have been demonstrated in the well-established single crystal silicon-on-insulator (SOI) platform because of its low transmission loss, tight optical confinement and high Kerr nonlinear coefficient n_2. More recently, polysilicon (p-Si) waveguides have emerged as an alternative platform, principally as they are much cheaper and more flexible to produce, so can be incorporated into a wider range of geometries [2] and architectures [3]. However, the high reported propagation losses in waveguides with small, few microns to hundreds of nanometer-sized, dimensions hinder their use in nonlinear applications.

In complement to the chip-based planar structures, low loss polysilicon waveguides can also be fabricated within the optical fiber platform using the molten core drawing (MCD) method, which is a derivative of the conventional fiber drawing approach [4]. However, silicon core fibers (SCFs) fabricated via the MCD method typically exhibit large core sizes (tens of microns) as it is difficult to produce continuous lengths of core with smaller dimensions owing to the high drawing temperatures and speeds [2, 5]. Thus, a modified tapering procedure has been introduced to scale down the cores of the MCD SCFs to diameters of a few micrometers, or less. Importantly, this post-processing method has also been shown to further improve the

#346882 https://doi.org/10.1364/OME.9.001271
Journal © 2019 Received 27 Sep 2018; revised 14 Nov 2018; accepted 14 Nov 2018; published 19 Feb 2019

Optical Materials EXPRESS

crystalline quality of the core material, resulting in a reduction in optical transmission losses in the telecom band from 12 dB/cm in 10 μm diameter as-drawn fibers, down to 3.5 dB/cm in a 1 μm tapered core fiber [6]. This combination of small core size and low loss has allowed for the first observation of nonlinear propagation in a polysilicon material, with the measured nonlinear parameters being comparable with those of single crystal silicon at the telecom wavelength of $\sim$ 1.55μm [7]. However, owing to the high nonlinear losses of crystalline silicon in this regime, recently there has been increased interest in their nonlinear properties in the mid-infrared, which is beyond the two-photon absorption (TPA) edge [8, 9]. Although measurements of the wavelength dependence of the TPA and Kerr nonlinearity have been reported in bulk materials and SOI waveguides [10–12], as of to date, there have been no reports for polysilicon waveguides and/or for SCFs fabricated via the MCD method.

In this paper, we extend the characterizations of the polycrystalline SCFs beyond the telecommunications window and present the first systematic investigation of the transmission properties of this fiber platform spanning from 1.5 to 2.5 μm. This range was specifically selected as it starts from the telecommunications band and continues across the TPA edge $\hbar\omega < E_{\mathrm{gi}}/2$, where E_{gi} is the indirect bandgap energy of crystalline silicon. A series of wavelength dependent measurements have been conducted using various continuous wave (CW) and short pulse laser sources to determine both the linear losses and the nonlinear transmission properties related to the β_{TPA} and n_2 parameters. This characterization provides useful information regarding the quality of our polysilicon core material as well as the dispersion of the $\mathrm{FOM_{NL}}$ in the vicinity of the TPA edge. By exploiting the low linear losses and the negligible nonlinear absorption for wavelengths beyond 2 μm, a broad continuum spanning from 1.8 μm to 3.4 μm is also generated. The results indicate the potential for SCFs to find use in nonlinear applications across the mid-infrared region where applications include spectroscopy, imagining and sensing.

2. Fabrication of tapered silicon fibers and experimental setup

The SCFs studied in this work were fabricated using the MCD technique described in [5]. A thin layer of calcium oxide (CaO) was introduced between the silicon rod and the outer silica cladding to act as a stress buffer, which also prevents oxygen in-diffusing from the cladding to the core during the high temperature draw process. The as-drawn SCFs are polycrystalline, with longitudinal crystal grain sizes on the order of a few millimeters, and have an outer cladding diameter of 377 μm and a core diameter of 30 μm. For nonlinear applications, SCFs with core sizes of a few micrometers or smaller are favored. Thus the as-draw SCFs are subsequently tapered using a Vytran tapering rig (GPX-3400) by slowly feeding the fiber into the hot zone and pulling it from the other end with a higher pulling speed. Various tapered fiber core waists can be produced by controlling the tapering ratio, filament power and pulling velocity. For the following investigations, a uniform waist region with a core diameter of 3 μm over a 1 cm length was selected. An optical microscope image of the tapered SCF is shown in the inset of Fig. 1(a). The silicon core is confirmed to be polycrystalline by Raman spectroscopy and X-ray diffraction measurements, which have been published in our previous work [6].

The optical transmission measurements were conducted using the experimental setup shown in Fig. 1(a). Two laser sources: (i) a fiber laser generating hyperbolic secant pulses with a 650 fs (FWHM) duration operating at 1.54 μm with a repetition rate of 40 MHz and (ii) a Ti:sappire pumped femtosecond optical parametric oscillator (OPO) for the mid-infrared measurements spanning 1.7 – 2.5 μm with a 200 fs (FWHM) duration and a repetition rate of 80 MHz, were employed to measure both the linear losses and nonlinear parameters over the wavelength range 1.5 – 2.5 μm. The light was launched into the core of the polycrystalline SCF using a silica microscope objective (L1) (NA = 0.85) with an average coupling loss $\sim$ 3.6dB (excluding Fresnel reflections) over the entire wavelength region and the output light was captured using another silica microscope objective lens (L2). Then the transmitted light was measured by

Optical Materials EXPRESS

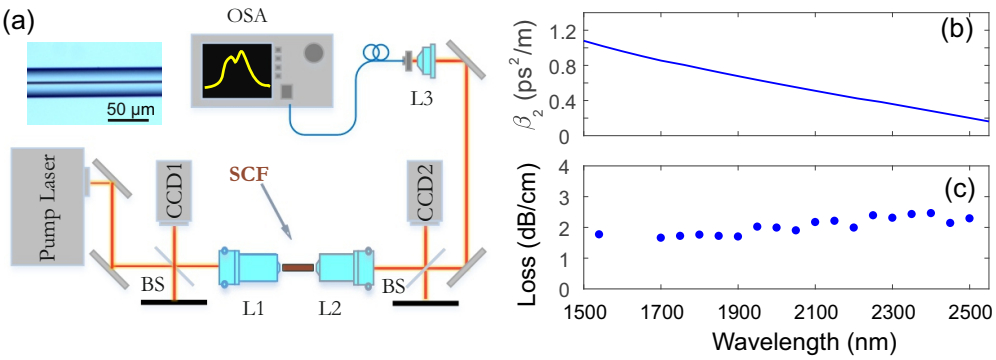

Fig. 1. (a) Schematic of the transmission setup. Beam-splitter (BS), microscope objective lenses (L1, L2 & L3), CCD Cameras (CCD1 & CCD2), optical spectrum analyser (OSA). Inset shows an optical microscope image of the tapered SCF, where the silicon core (black) is clearly visible. (b) Calculated dispersion profile of the polycrystalline SCF as a function of wavelength. (c) Linear loss measurements as a function of wavelength.

either a power meter or focused to an optical spectrum analyzer (OSA: Yokagawa AQ 6375) using another microscope objective lens (L3) (NA = 0.65). The pump power coupled into the polycrystalline SCF was controlled by a variable attenuator (ND filter). CCD cameras were employed to ensure efficient coupling into the center of the core so that the fundamental mode was primarily excited [13].

As the refractive index for polysilicon is not well documented, the wavelength dependent group velocity dispersion (GVD) parameter β_2 of the fundamental mode was estimated by using parameters from the Sellmeier equation for c-Si [14]. As shown in Fig. 1(b), this SCF exhibits normal dispersion across the entire wavelength range: 1.5 μm to 2.5 μm. This is because the waveguide dispersion of our micron-sized core is not sufficient to compensate for the large normal material dispersion of the high index silicon core. However, this is advantageous for our nonlinear characterization as it ensures that the nonlinear propagation will be governed simply by self-phase modulation (SPM). Furthermore, as the 1 cm fiber length is shorter than the dispersion length $L_D = T_0^2/|\beta_2|$ at all the wavelengths, we can be sure that the nonlinear effects dominate the high power transmission measurements, i.e., $L_{NL} = 1/\gamma P_0 \ll L_D$. In this study, we neglect contributions from higher order dispersion as the SCF exhibits relatively large normal GVD over the entire wavelength region, thus their impact on the pulse propagation and spectral broadening is minimal.

3. Optical transmission properties

3.1. Linear propagation loss

The linear propagation losses of the SCFs were measured using the cut-back method as described in [15]. In order to avoid the effects of nonlinear absorption when using the pulsed lasers, the average launch power was kept below 100 μW. To verify this value, additional measurements were conducted with a 1.55 μm CW diode, which returned the same loss as our high power fiber laser, confirming that the nonlinear absorption was indeed negligible for these input powers. The loss values stay consistently low at values around 1 – 2.5 dB/cm over the entire wavelength range as shown in Fig. 1 (c). These loss values are comparable with those of SOI waveguides over the same wavelength region [16] and present a unique opportunity to investigate the nonlinear properties of this material, and the MCD SCFs. Although the losses measured here are in agreement with our previous work, indicating that the crystallinity of the core is high [6], reducing

Optical Materials EXPRESS

the losses even further would greatly improve the practicality of these fibers and the material properties are an ongoing study in the tapered SCFs.

3.2. Nonlinear absorption in the mid-infrared regime

Characterization of the TPA parameter was performed by measuring the saturation of the output pulses as a function of increasing input power. Our experimental setup employed the same lasers as in Section 3.1, but operating at higher powers for nonlinear measurements. Fig. 2(a) plots the results of the output power as a function of coupled input peak intensity for selected pump wavelengths across the TPA window. For all wavelengths up to 2.15 μm, it is obvious that the output powers saturate due to the strong nonlinear absorption caused by TPA when the coupled peak intensity exceeds 2 GW/cm^2. In contrast, the largely linear trend exhibited for transmission at 2.35 μm, which continues up to an input peak intensity of $\sim$ 8 GW/cm^2, indicates that TPA is essentially negligible at this wavelength. Although three-photon absorption (3PA) can become significant at wavelengths beyond the TPA edge, the peak intensity in our measurements are insufficient for the observation of the power saturation caused by 3PA [17].

As discussed in [18], when dispersion can be neglected, the transmitted pump power through the fiber can be described by a simplified nonlinear Schrödinger equation (NLSE) coupled to the rate equation for TPA generated free-carriers:

$$\frac{\partial I(z,t)}{\partial z} = -\alpha_l I(z,t) - \beta_{\mathrm{TPA}} I^2(z,t) - \sigma_{\mathrm{FCA}} N_c(z,t) I(z,t), \tag{1}$$

$$\frac{\partial N_c(z,t)}{\partial t} = \frac{\beta_{\mathrm{TPA}}}{2h\nu_0} I^2(z,t) - \frac{N_c(z,t)}{\tau_c}. \tag{2}$$

Here $I(z,t)$, α_l, σ_{FCA}, N_c, and τ_c represent the pulse intensity, linear loss, free-carrier absorption (FCA) coefficient, free-carrier density, and the carrier lifetime, respectively. To determine the values of β_{TPA}, we fit the experimental data for all wavelengths using the coupled equations, with the remaining material parameters estimated from the single crystal values. This fitting method, which includes the free carrier contributions, is more generalised than estimating the

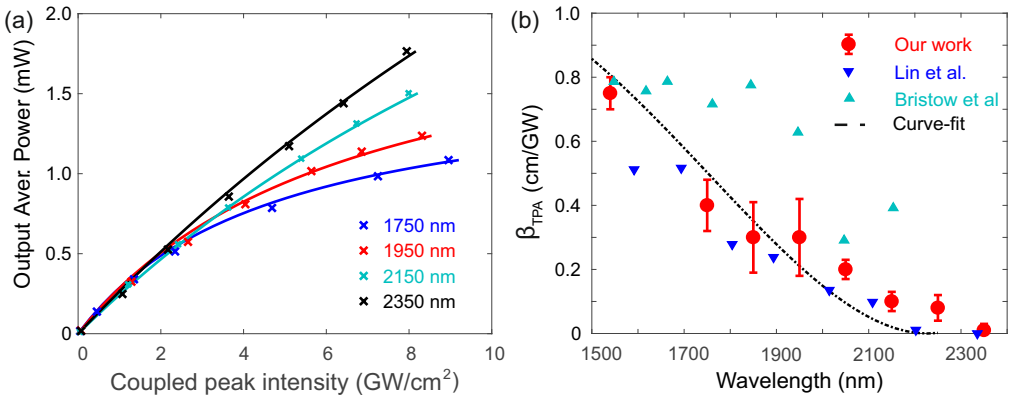

Fig. 2. (a) Nonlinear absorption measurements for different wavelengths. The solid curves are simulated fits to the data for the corresponding wavelength given in the legend. (b) Measured TPA parameter as a function of wavelength extracted from Fig. 2(a), together with data points from previous measurements [10, 11] in bulk silicon as labeled. Error bars represent the uncertainty in the input powers.

Optical Materials EXPRESS

TPA parameters from the slope of the reciprocal transmission (1/T or P_{in}/P_{out}) versus input peak power [12]. However, as the typical carrier lifetime $\tau_c \sim 100$ ns for the silicon core material is much longer than the femtosecond pulse durations used in the measurements, we expect the free carrier contributions to have a limited influence on the pulse propagation. Both methods returned similar TPA parameters in our case, indicating that the free carrier contributions was indeed negligible. The resulting curves are plotted as the solid lines in Fig. 2(a), from which we can obtain the TPA parameters presented in Fig. 2(b) (red circles). These results show that β_{TPA} initially drops from 0.75 cm/GW down to 0.1 cm/GW as the wavelength increases from the telecom window to the mid-infrared regime ($1.54 - 2.15\ \mu$m), then eventually begins to plateau at a negligible value as the wavelength approaches the edge of the TPA window ($2.25\ \mu$m). The β_{TPA} tends to zero for $\lambda > 2.25\ \mu$m, where the sum of the energies of two photons is no longer sufficient to span the bandgap. The trend of decreasing β_{TPA} seen in Fig. 2(b) is what we would expect across this regime, and the results are in good agreement with those reported previously in the literature for bulk silicon [10, 11]. The slight differences for the longer wavelengths may stem from the polycrystalline nature of our core material, as there will be material defects at the grain boundaries. However, it is worthwhile to note that our experimental measurements are in very good agreement with the theoretical fits based on calculations of Garcia and Kalyanaraman [19], as shown in the dashed line in Fig. 2(b).

3.3. SPM induced spectral evolution

The spectral broadening induced by SPM was then studied to determine the values of the Kerr coefficient n_2 over this wavelength range. As in the nonlinear absorption measurements, for these experiments high input peak powers were used, but this time the output spectra of the pulses were monitored on the OSA. The measured SPM spectra are shown in Fig. 3 for selected wavelengths from $1.55 - 2.35\ \mu$m. For each pump wavelength, the output transmission spectra were recorded at both low and high input peak intensities, as designated by the legends. Here, the results obtained with the low input intensities are essentially free from nonlinear propagation and are included as an indicator of the bandwidth of the input pulse, as a means to determine the size of the initial negative frequency chirp on the pulses, which are not transform-limited. The chirp was not found to vary dramatically over this wavelength range and had a value of $C \sim -1.1$ for all wavelengths [20]. The high intensity results are then used to illustrate the strong spectral broadening due to the large Kerr nonlinearity of the silicon core, with bandwidths (at -30 dB) of more than 300 nm obtained for all wavelengths. It is also worth noting that the lack of clear SPM induced modulation on these spectra is due to the initial chirp on the pulses and the noise on the input OPO spectra.

The magnitude of the Kerr coefficient n_2 for each central wavelength is subsequently estimated by fitting the spectral broadening with the solutions to the full NLSE equation:

$$\frac{\partial A(z,t)}{\partial z} = -\frac{i\beta_2}{2}\frac{\partial^2 A(z,t)}{\partial t^2} + i\gamma|A(z,t)|^2 A(z,t) - \frac{1}{2}(\alpha_l + \sigma_f)A(z,t) \tag{3}$$

coupled to Eq. 2 with the predetermined loss parameters and remaining material parameters. Here $A(z,t)$, β_2, γ, α_l, and σ_f represent the slowly varying pulse envelope, group velocity dispersion (GVD), nonlinear parameter, linear loss, and the free carrier contribution, respectively. A complex nonlinear parameter is included to account for both the Kerr and TPA contributions: $\gamma = k_0 n_2/A_{eff} + i\beta_{TPA}/2A_{eff}$, where A_{eff} is the effective mode area (note: $A_{eff} \sim 3.7 \times 10^{-12}$ m^2 for all wavelengths). Similarly, the free carrier contribution is also complex: $\sigma_f = \sigma(1 + i\mu)N_c$, where σ is the FCA coefficient and μ governs the free-carrier dispersion (FCD).

As shown in Fig. 3, the simulated fits (black dash lines) are in reasonable agreement with the measured spectra at the same input peak intensity. To quantify the spectral comparison

Optical Materials EXPRESS

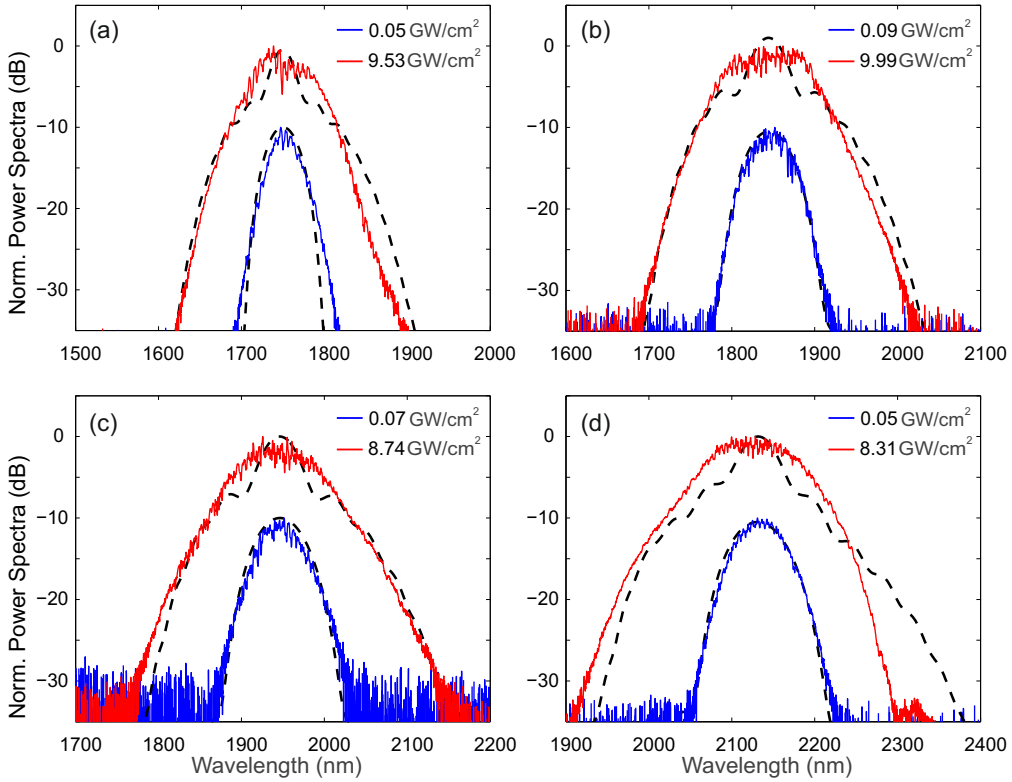

Fig. 3. Experimental power-dependent transmission spectra as a function of pump center wavelength: (a) 1750 nm, (b) 1850 nm, (c) 1950 nm, and (d) 2150 nm. The dashed lines are numerical fits obtained by solving the generalized NLSE [18]. The normalized spectra are offset for clarity.

between the simulations and measurements, Table 1 lists the bandwidths (at -20 dB) of the measured spectra with simulated fits for these pump wavelengths. As we can see from the table, the measured spectra are well matched to the simulations in terms of bandwidth, indicating the nonlinear coefficient n_2 used in the simulations is close to the values of the SCF core material at the corresponding wavelength.

Table 1. -20 dB bandwidth for selected pump wavelengths.

Wavelength (nm)	1750	1850	1950	2050	2150	2250	2350*
Experimental bandwidth (nm)	192	250	281	281	303	321	168
Simulated bandwidth (nm)	218	264	280	285	326	318	178

*Bandwidth was taken at - 10 dB due to OSA's maximum measurable wavelength of 2400 nm.

The corresponding values of n_2 are plotted in Fig. 4(a), which show that as the input pulse wavelength shifts across the TPA edge, the n_2 value first increases slightly up to a value of 1.0×10^{-13} cm^2/W at 1.75 μm, then drops to a modest value of 0.7×10^{-13} cm^2/W at 2.35 μm. This trend is as expected from the nonlinear Kramers-Krönig relation, where the values of n_2 increase for wavelengths moving away from the band edge, until they reach a peak just short

Optical Materials EXPRESS

of the TPA edge. The n_2 dispersion profile is consistent with the measurements by Bristow *et al.* [10] and the theoretical predictions of Hon *et al.* [21], where the values of n_2 peak at approximately the same wavelength. However, although the measured Kerr coefficient n_2 of the polycrystalline SCF is of the same order of magnitude as previously reported for single crystal materials, it is slightly lower, which may be attributed to the different crystal orientations present in the cores [22]. We note that the error bars represent experimental uncertainties originating from intensity fluctuations in the laser power and variations in the beam shape induced by tuning the OPO.

3.4. Nonlinear figure of merit and continuum generation

As a final step, the nonlinear parameters β_{TPA} and n_2 were used to investigate the dispersion of the $\mathrm{FOM_{NL}}$(defined as $n_2/\lambda\beta_{\mathrm{TPA}}$), plotted in Fig. 4(b). This figure clearly shows that despite the decrease in n_2 at the longer wavelengths, the dramatic reduction in β_{TPA} results in a monotonic increase in the $\mathrm{FOM_{NL}}$. The value of the $\mathrm{FOM_{NL}}$ at 1.55 μm for this polycrystalline SCF is fairly modest $\sim$ 0.36, though is comparable to previous reports in SOI waveguides [11], but the increasing trend indicates that these fibers should be suitable for nonlinear applications at wavelengths above 2 μm. However, we note that the TPA definition for the $\mathrm{FOM_{NL}}$ is not entirely accurate for the final measurement at 2.35 μm, as it is beyond the TPA edge, and a more accurate definition would be based on the 3PA parameter as, $n_2/\lambda\beta_{3\mathrm{PA}}I$, where I is the intensity inside the nonlinear medium. Using data for the 3PA parameter of single crystal silicon from the literature [17], the 3PA $\mathrm{FOM_{NL}}$ is plotted as the red square in Fig. 4(b) for comparison, where $I \sim 1\,\mathrm{GW/cm^2}$. Although this modified value is lower, it is clear that the $\mathrm{FOM_{NL}}$ continues its upward trend, so that one can expect higher nonlinear performance in the SCFs at longer

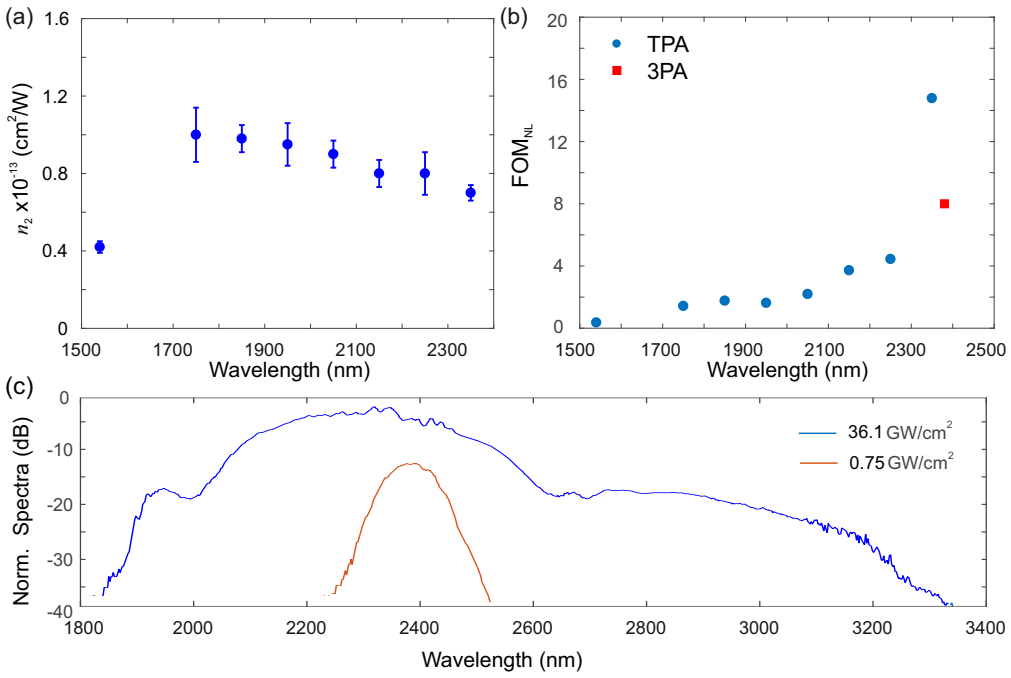

Fig. 4. (a) Wavelength dependence of the Kerr nonlinear coefficient n_2 for the tapered SCF. Error bars represent the uncertainty in the input pulses. (b) Wavelength dispersion of the $\mathrm{FOM_{NL}}$. (c) Continuum generated by pumping in the normal dispersion regime.

Optical Materials EXPRESS

wavelengths.

As a final demonstration of the optical quality of our polycrystalline SCFs, Fig. 4(c) shows a supercontinuum spectrum generated when pumped with an input pulse at $\lambda_p = 2.4\,\mu$m and an intensity of $36.1\,\mathrm{GW/cm^2}$. The bandwidth of the spectrum is $\sim 1600\,$nm at the $-40\,$dB level, corresponding to ~ 0.9 of an octave. Although this is not the broadest spectrum that has been generated in a crystalline silicon waveguide, to the best of our knowledge, it is the broadest that has been generated in the normal dispersion regime. Significantly, continuum spectra generated in the normal dispersion regime are often favoured for applications in spectroscopy and metrology as their flatness and coherence is better [23]. This is because SPM dominates the broadening mechanism, so that phase noise introduced by processes such as four-wave mixing or modulation instability is kept to a minimum. However, future work will look to broaden the continuum further by fabricating SCFs with smaller core diameters to access the anomalous dispersion region. Alternatively, more complex fiber geometries and/or material systems could enable new possibilities. For example, fibers with tapered core dimensions could be designed to phase match multiple nonlinear processes or germanium could be added to the core material to increase the nonlinear coefficients and extend the transmission to longer mid-infrared wavelengths [24]. Eventually, when fully integrated with conventional mid-infrared fibers and components to improve the robustness of the system [25], we expect these SCFs will find wide-ranging applications in areas that require wavelength conversion in this important spectral band.

4. Conclusion

We have characterized both the linear and nonlinear transmission properties of our MCD SCFs from telecom wavelengths up to the TPA edge in the mid-infrared regime. The dispersion curves obtained for the TPA and nonlinear refractive index are in good qualitative agreement with previous reports for single crystal silicon, indicating the high quality of the polysilicon core materials. The large spectral broadening measured for wavelengths beyond $2\,\mu$m suggest that polycrystalline SCFs are a viable platform for nonlinear applications within the short-wave and mid-infrared regimes, where applications include free-space communications, gas detection and medical diagnostics. We expect that continued efforts to understand the properties of these fibers and their highly nonlinear core material will help to establish their use in wide ranging areas of research.

Funding

Engineering and Physical Sciences Research Council (EPSRC) (EP/P000940/1); National Natural Science Foundation of China (NSFC) (61705072); Natural Science Foundation of Hubei Province (2017CFB133); the Norwegian Research Council (NORFAB); the J.E. Sirrine Foundation.

Acknowledgments

All data supporting this study are openly available from the University of Southampton repository at https://doi.org/10.5258/SOTON/D0710 [26].

References

1. J. Leuthold, C. Koos, and W. Freude, "Nonlinear silicon photonics," Nat. Photonics **4**(8), 535–544 (2010).
2. J. Ballato, T. Hawkins, P. Foy, R. Stolen, B. Kokuoz, M. Ellison, C. McMillen, J. Reppert, A. M. Rao, M. Daw, S. Sharma, R. Shori, O. Stafsudd, R. R. Rice, and D. R. Powers, "Silicon optical fiber," Opt. Express **16**(23), 18675-18683 (2008).
3. J. S. Orcutt, S. D. Tang, S. Kramer, K. Mehta, H. Li, V. Stojanović, and R. J. Ram, "Low-loss polysilicon waveguides fabricated in an emulated high-volume electronics process," Opt. Express **20**(7), 7243-7254 (2012).
4. A. C. Peacock, U. J. Gibson, and J. Ballato, "Silicon optical fibres - past, present, and future," Adv. Phys.: X **1**, 114-127 (2016).

Optical Materials EXPRESS

5. E. F. Nordstrand, A. N. Dibbs, A. J. Eråker, and U. J. Gibson, "Alkaline oxide interface modifiers for silicon fiber production," Opt. Mater. Express **3**(5), 651-657 (2013).
6. Y. Franz, A. F. J. Runge, H. Ren, N. Healy, K. Ignatyev, M. Jones, T. Hawkins, J. Ballato, U. J. Gibson, and A. C. Peacock, "Material properties of tapered crystalline silicon core fibers," Opt. Mater. Express **7**(6), 2055-2061 (2017).
7. F. H. Suhailin, L. Shen, N. Healy, L. Xiao, M. Jones, T. Hawkins, J. Ballato, U. J. Gibson, and A. C. Peacock, "Tapered polysilicon core fibers for nonlinear photonics," Opt. Lett. **41**(7) 1360-1363 (2016).
8. X. P. Liu, R. M. Osgood, Y. A. Vlasov, and W. M. J. Green,"Mid-IR optical parametric amplifier using silicon nanophotonic waveguides," Nat. Photonics **4**(8), 557–560 (2010).
9. S. Zlatanovic, J. S. Park, S. Moro, J. M. C. Boggio, I. B. Divliansky, N. Alic, S. Mookherjea, and S. Radic, "Mid-IR wavelength conversion in silicon waveguides using ultracompact telecom-band-derived pump source," Nat. Photonics **4**(8), 561–564 (2010).
10. A. D. Bristow, N. Rotenberg, and H. M. Van Driel, "Two-photon absorption and Kerr coefficients of silicon for 850 − 2200 nm," Appl. Phys. Lett. **90**(19), 191104 (2007).
11. Q. Lin, J. Zhang, G. Piredda, R. W. Boyd, P. M. Fauchet, and G. P. Agrawal, "Dispersion of silicon nonlinearities in the near infrared region," Appl. Phys. Lett. **90**(2), 191104 (2007).
12. X. P. Liu, J. B. Driscoll. J. I. Dadap, R. M. Osgood, S. Assefa, Y. A. Vlasov, and W. M. J. Green, "Self-phase modulation and nonlinear loss in silicon nanophotonic wires near the mid-IR two-photon absorption edge," Opt. Express **19**(8), 7778-7789 (2011).
13. A. C. Peacock, P. Mehta, P. Horak, and N. Healy, "Nonlinear pulse dynamics in multimode silicon core optical fibers," Opt. Lett. **37**(16), 3351–3353 (2012).
14. H. H. Li, "Refractive index of silicon and germanium and its wavelength and temperature derivatives," J. Phys. Chem. Ref. Data **9**, 561–658 (1980).
15. L. Lagonigro, N. Healy, J. R. Sparks, N. F. Baril, P. J. A. Sazio, J. V. Badding, and A. C. Peacock, "Low loss silicon fibers for photonics applications," Appl. Phys. Lett. **96**(4), 041105 (2010).
16. M.-S. Rouifed, C. G. Littlejohns, G. X. Tina, Q. Haodong, T. Hu, Z. Zhang, C. Liu, G. T. Reed, and H. Wang, "Low loss SOI waveguides and MMIs at the MIR wavelength of 2 μm," IEEE Photonics Technol. Lett. **28**(24), 2827-2829 (2016).
17. F. Gholami, S. Zlatanovic, A. Simic, L. Liu, D. Borlaug, N. Alic, M. Nezhad, Y. Fainman, and S. Radic, "Third-order nonlinearity in silicon beyond 2350 nm," Appl. Phys. Lett. **99**(8), 081102 (2011).
18. P. Mehta, N. Healy, N. F. Baril, P. J. A. Sazio, J. V. Badding, and A. C. Peacock, "Nonlinear transmission properties of hydrogenated amorphous silicon core optical fibers," Opt. Express **18**(16), 16826–16831 (2010).
19. H. Garcia and R. Kalyanaraman,"Phonon-assisted two-photon absorption in the presence of a dc-field: the nonlinear Franz-Keldysh effect in indirect gap semiconductors," J. Phys. B **39**(12), 2737-2746 (2006).
20. L. Shen, N. Healy, P. Mehta, T. D. Day, J. R. Sparks, J. V. Badding, and A. C. Peacock, "Nonlinear transmission properties of hydrogenated amorphous silicon core fibers towards the mid-infrared regime," Opt. Express **21**(11), 13075–13083 (2013).
21. N. Hon, R. Soref, and B. Jalali, "The third-order nonlinear optical coefficients of Si, Ge, and $Si_{1-x}Ge_x$ in the midwave and longwave infrared," J. Appl. Phys. **110**, 011301 (2011).
22. J. Zhang,"Anisotropic nonlinear response of silicon in the near-infrared region," Appl. Phys. Lett. **91**(7), 071113 (2007).
23. A. M. Heidt, "Pulse preserving flat-top supercontinuum generation in all-normal dispersion photonic crystal fibers," J. Opt. Soc. Am. B **27**(3), 550-559 (2010).
24. D. A. Coucheron, M. Fokine, N. Patil, D. W. Breiby, O. T. Buset, N. Healy, A. C. Peacock, T. Hawkins, M. Jones, J. Ballato, and U. J. Gibson, "Laser recrystallization and inscription of compositional microstructures in crystalline SiGe-core fibres," Nat. Commun **7**, 16265 (2016).
25. H. Ren, O. Aktas, Y. Franz, A. F. J. Runge, T. Hawkins, J. Ballato, U. J. Gibson, and A. C. Peacock, "Tapered silicon core fibers with nano-spikes for optical coupling via spliced silica fibers," Opt. Express **25**(20), 24157-24163 (2017).
26. L. Shen, H. Ren, and A. Peacock, "Dataset for Nonlinear optical properties of polycrystalline silicon core fibers from telecom wavelengths into the mid-infrared spectral region," University of Southampton (2018), https://doi.org/10.5258/SOTON/D0710.